Hindawi
Applied Bionics and Biomechanics
Volume 2018, Article ID 1308465, 10 pages
https://doi.org/10.1155/2018/1308465

Research Article

Design and Mechanical Analysis of Bionic Foldable Beetle Wings

Caidong Wang,[1,2] **Chen Wang**,[1] **Yu Ning**,[1] **Lumin Chen**,[1] **and Xinjie Wang**[1]

[1]*College of Mechanical and Electrical Engineering, Zhengzhou University of Light Industry, Zhengzhou 450002, China*
[2]*Henan Key Laboratory of Intelligent Manufacturing of Mechanical Equipment, Zhengzhou 450002, China*

Correspondence should be addressed to Caidong Wang; vwangcaidong@163.com

Received 20 April 2018; Accepted 4 July 2018; Published 9 August 2018

Academic Editor: Laurence Cheze

In order to improve the flight performance of collapsible aircrafts, a novel mechanism of bionic foldable wings of beetle is designed based on the four-plate mechanism theory. The folding and unfolding movements of the bionic foldable wings are driven by motor and torsion hinges. Based on the D-H method, a kinematic model of wings is established to analyze the dihedral angle of adjacent plates. The folding ratio of an area in different plate creasing angles has been derived and calculated. Utilizing the kinematic and static models produced, as well as considering the folding ratio and output motor torque, the optimal physical parameters of folding wings are obtained. Dynamic models of rigid and flexible wings were established using ADAMS, and a motion simulation was performed. The relationship between dihedral angle and torque during the folding process of both rigid and flexible wings was obtained. The results provide a better understanding of the folding mechanism through the formulation of rigid-flexible wing analysis, as well as demonstrating a novel design of insect-mimicking artificial wings for small aerial vehicles.

1. Introduction

Bionics is one of the most important examples of researchers seeking better inventions and engineering designs. The flying ability of birds, insects, and other creatures is amazing. The study of flight principles observed in nature can greatly improve the performance of existing aircrafts and promote the development of new and unique aircrafts [1–3]. Compared with the traditional aircrafts, flapping-wing air vehicles have advantages such as simpler design, lower noise, higher efficiency, and better environmental protection [4–6]. However, observation of insect flight is a relatively recent field of study. Beetles (Coleoptera) can drill into soil and water after storing their flexible wings under their sheath wings. The folding ratio of these flexible wings is relatively large [7]. At present, the bionic design of foldable wings is mainly concentrated structural considerations, which restricts the improvement of motion performance [8]. Therefore, it is important to study on the bionic design and the motion mechanism of flexible foldable wings.

The good flight characteristics of the foldable wings have attracted a significant number of researchers. Muhammad et al. [9] divided the membrane structure of the *Allomyrina dichotoma* beetle wings. The characteristics of folding and unfolding of wings were analyzed. Two types of artificial wings driven by a shape memory alloy with 5 V, 1.5 A power supply were developed. Truong et al. [10] used a double four-bar mechanism for the folding of artificial wings, but the change of angle between the two main lines of wings was driven manually. Based on uniform velocity rigidity model, Rui et al. [11] obtained a new model of flapping wings of variable velocity by adding the influence of the change of the flapping rate and the change of the wing shape. This flapping model more closely captures bird wing flexibility. Zhenjun et al. [12] used the Lagrange method to infer the coupling equation of rigid-elastic deformations of flexible aircraft. Cheng [13] studied the deformation characteristics of flying wings of dragonfly using a projected sinusoidal grid method. Ha et al. [14] successfully developed a method based on a minitensile test system and the DIC method to measure Young's modulus and Poisson's ratio of the membrane of the hind wing of the *Allomyrina dichotoma* beetle. While most studies consider wingbeat kinematics critical to lift generation, few address the shape and mechanical properties of the wings themselves [15, 16]. Recent discoveries in the field of flapping-wing aerodynamics have demonstrated that

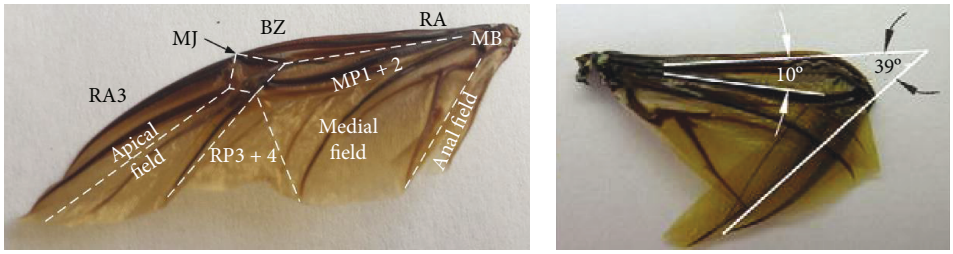

(a) Creases of the hind wings (b) Folding state of the hind wings

Figure 1: Hind wing shape analysis of *Allomyrina dichotoma* beetle.

flexible wings can generate more lift than rigid wings. Ghommem et al. [16] used the unsteady vortex lattice method together with a gradient-based optimizer to obtain optimized wing shapes that give maximum efficiency. This study also found that the optimal wing shapes are highly dependent on reducing the wingbeat frequency. Tay [17] performed 3D simulations to determine the effects of prescribed deformation on different types of wings under various flapping configurations. Bluman and Kang [18] found that the flexible wings require 32%–94% less power than rigid wings.

Haas and Wootton and Haas and Beutel proposed the four-board model for the folding and unfolding of insect hind wings [19, 20] but did not explain how to achieve it through mechanisms. Based on the four-plate model theory proposed by Haas and Wootton and Haas and Beutel, the mechanism of bionic foldable flexible wings of the beetle is designed in this paper. The mechanism of the foldable wings is driven by a motor and torsion hinge. The dynamic model of the rigid and flexible wings is established using ADAMS, and a motion simulation of bionic foldable wings is performed.

2. The Design of the Mechanism of Foldable Wings

The folding and unfolding configuration of the *Allomyrina dichotoma* beetle hind wings is shown in Figure 1. The hind wings are composed of the apical field, middle field, anal field, and wing veins. By observing the process of unfolding and folding of the unicorn hind wings, there are five creases in the folding process of the hind wings, as shown by the dotted line in Figure 1. Due to the area in the anal field that is smaller, its effect can be ignored. Then, the four creases of the hind wing intersect with one point.

During the wing folding process, elastic energy is stored in resilin, a rubber-like substance [20]. Resilin can be found at some locations in a hind wing, such as medial bridge (MB), bending zone (BZ), and marginal joint (MJ). But it is very difficult to imitate the biological characteristics of resilin to drive the hind wings to achieve folding and unfolding motion. Through an analysis of the physical form and movement of the *Allomyrina dichotoma* beetle, combined with the theory of mechanics, a model of the bionic wings is established. The model is shown in Figure 2.

The mechanism of foldable wings consists of four plates with 1 degree of freedom. The adjacent wing plates are

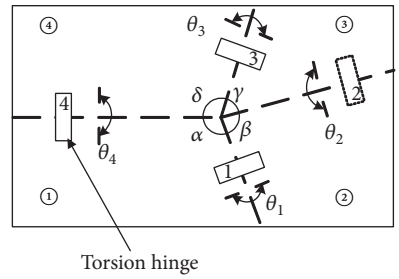

Figure 2: Schematic diagram of wings.

connected by torsion hinges, which are made of electroactive polymer (EAP) material. The folding of the hind wings is driven by the motor with elastic rope and unfolding by the elastic driving force of the electroactive polymer (EAP) torsion hinge. The creasing angle relationships for each plate of the wings are $\delta + \beta = \pi$ and $\gamma + \alpha = \pi$. The angle of adjacent plates as the dihedral angle θ is shown in Figure 1. The wing plates are connected by torsion hinges. Plate ④ is connected to the aircraft body at the base. Plate ③ is active against the elastic force of the torsion hinges and is rotated toward plate ④ and is driven by the motor. Plates ① and ② are driven by the torsion hinges as followers. The principle of the foldable wings is that when the wings are folding, the motor drives the torsion hinges to bend and drives the wings to complete the folding movement. When the wings are unfolding, the wings are driven by the elastic potential of the torsion hinges themselves.

Folding performance is a key factor to consider when designing a folding wing mechanism. Under the constraint of satisfying the output motor torque, the folding ratio of wings is given priority. In general, the design of the folding mechanism of wings should satisfy the following principles:

(1) The structure of wings should be simple, small in size, and lightweight.

(2) The creasing angle of adjacent wing plates should be reasonably designed in order to meet the folding ratio and motor torque requirements.

(3) The torsion hinges between the plates should be locked in the movement, thereby avoiding unwanted relative displacement of the plates.

(4) In order to avoid coupling motion between the plates, the movement of folding and unfolding of wings should be continuous and smooth.

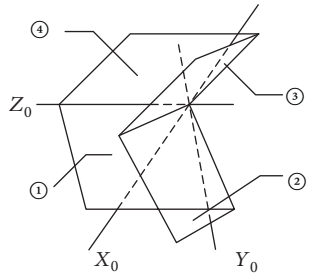

Figure 3: Schematic diagram of folding wings.

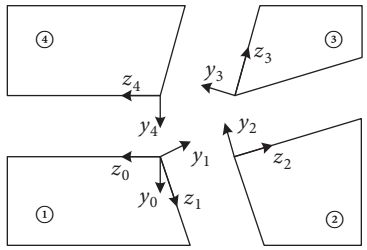

Figure 4: Simplified kinematics model.

In order to ensure adequate transmission performance, it is necessary to reasonably design the size and angle of plates and avoid dead spots to prevent becoming stuck in the process of the movement. As such, the requirements $\delta > 90^\circ$ and $\gamma < 90^\circ$ should be met.

The function of torsion hinges is to connect and fix the plates. In the process of flapping, the wings are in an expanded state and the bending moment, torque, and shear stress caused by the aerodynamic load on the airfoil are transmitted as concentrated force through the torsion hinges. At this moment, the folding wing mechanism only needs to withstand its own gravity and air resistance.

3. Characteristics of Foldable Wings

3.1. Analysis of Kinematics. The present simplified kinematic model of foldable wings is shown in Figure 3. The coordinate system of each plate is set up by the D-H parameter method, as shown in Figure 4. The coordinate system parameters of the foldable wings are shown in Table 1.

Table 1: D-H parameter of plates.

i	a_{i-1}	α_{i-1}	d_i	θ_i
1	0	α	0	θ_1
2	0	β	0	θ_2
3	0	γ	0	θ_3
4	0	δ	0	θ_4

According to the kinematic homogeneous transform theory, the transformation matrix of adjacent plate ② is

$$
\begin{aligned}
{}^2_1\mathbf{T} &= \begin{bmatrix} c\beta & s\beta c\theta_1 & -s\beta s\theta_1 & 0 \\ -s\beta & c\beta c\theta_1 & -c\beta s\theta_1 & 0 \\ 0 & s\theta_1 & c\theta_1 & 0 \\ 0 & 0 & 0 & 1 \end{bmatrix}, \\
{}^1_4\mathbf{T} &= \begin{bmatrix} c\alpha & s\alpha c\theta_4 & -s\alpha s\theta_4 & 0 \\ -s\alpha & c\alpha c\theta_4 & -c\alpha s\theta_4 & 0 \\ 0 & s\theta_4 & c\theta_4 & 0 \\ 0 & 0 & 0 & 1 \end{bmatrix}, \\
{}^2_3\mathbf{T} &= \begin{bmatrix} c\gamma & -s\gamma & 0 & 0 \\ s\gamma c\theta_2 & c\gamma c\theta_2 & -s\theta_2 & 0 \\ s\gamma s\theta_2 & c\gamma s\theta_2 & c\theta_2 & 0 \\ 0 & 0 & 0 & 1 \end{bmatrix}, \\
{}^3_4\mathbf{T} &= \begin{bmatrix} c\delta & -s\delta & 0 & 0 \\ s\delta c\theta_3 & c\delta c\theta_3 & s\theta_3 & 0 \\ -s\delta s\theta_3 & -c\delta s\theta_3 & c\theta_3 & 0 \\ 0 & 0 & 0 & 1 \end{bmatrix},
\end{aligned} \tag{1}
$$

where $s\theta_i = \sin\theta_i$ and $c\theta_i = \cos\theta_i$.

From the space position constraint of plate ②, we can get ${}^2_1\mathbf{T}{}^1_4\mathbf{T} = {}^2_4\mathbf{T} = {}^2_3\mathbf{T}{}^3_4\mathbf{T}$.

$$
\begin{aligned}
\mathbf{A} = {}^2_4\mathbf{T} = {}^2_1\mathbf{T}{}^1_4\mathbf{T} &= \begin{bmatrix} c\alpha c\beta - s\alpha s\beta c\theta_1 & c\theta_4(c\beta s\alpha + c\alpha s\beta c\theta_1) - s\beta s\theta_1 s\theta_4 & -s\theta_4(c\beta s\alpha + c\alpha s\beta c\theta_1) - s\beta c\theta_4 s\theta_1 & 0 \\ -c\alpha s\beta - c\beta s\alpha c\theta_1 & -c\theta_4(s\alpha s\beta - c\alpha c\beta c\theta_1) - c\beta s\theta_1 s\theta_4 & s\theta_4(s\alpha s\beta - c\alpha c\beta c\theta_1) - c\beta c\theta_4 s\theta_1 & 0 \\ -s\alpha s\theta_1 & c\theta_1 s\theta_4 + c\alpha c\theta_4 s\theta_1 & c\theta_1 c\theta_4 - c\alpha s\theta_1 s\theta_4 & 0 \\ 0 & 0 & 0 & 1 \end{bmatrix}, \\
\mathbf{B} = {}^2_4\mathbf{T} = {}^2_3\mathbf{T}{}^3_4\mathbf{T} &= \begin{bmatrix} c\delta c\gamma - s\delta s\gamma c\theta_3 & -c\gamma s\delta - c\delta s\gamma c\theta_3 & -s\gamma s\theta_3 & 0 \\ s\delta(s\theta_2 s\theta_3 + c\gamma c\theta_2 c\theta_3) + c\delta s\gamma c\theta 2 & c\delta(s\theta_2 s\theta_3 + c\gamma c\theta_2 c\theta_3) - s\delta s\gamma c\theta_2 & c\gamma c\theta_2 s\theta_3 - c\theta_3 s\theta_2 & 0 \\ c\delta s\gamma s\theta_2 - s\delta(c\theta_2 s\theta_3 - c\gamma c\theta_3 s\theta_2) & -c\delta(c\theta_2 s\theta_3 - c\gamma c\theta_3 s\theta_2) - s\delta s\gamma s\theta_2 & c\theta_2 c\theta_3 + c\gamma s\theta_2 s\theta_3 & 0 \\ 0 & 0 & 0 & 1 \end{bmatrix}.
\end{aligned} \tag{2}
$$

Due to the homogeneous transformation matrix $\mathbf{A} = \mathbf{B}$, it is obtained that the relations for θ_1, θ_2, θ_3, and θ_4 are

$$\begin{aligned}&\theta_1 = \theta_3,\\&\theta_2 = \theta_4\\&\quad = \frac{c\gamma s\delta + c\theta_3 s\gamma c\delta}{s\delta s\theta_3 + (s\gamma c\delta + c\theta_3 c\gamma s\delta)(s\gamma s\delta - c\theta_3 c\gamma c\delta + c\theta_3)/(s\theta_3 c\gamma - s\theta_3 c\delta)}.\end{aligned} \tag{3}$$

The kinematic model of foldable wings was programmed using MATLAB software. The simulation results of the folding and unfolding movement of wings are shown in Figure 5. When angle θ_1 moves along the desired trajectory, the curve of angle θ_2 can be obtained according to the above mathematical model. In the movement of folding, the motion of θ_2 is smooth between 180 ° and 130 °. The change of angle speeds up between 130° and 0°. That is, the trend of the change in angle in the folding process is to be slow and then fast. In the movement of unfolding, the change of θ_2 is faster between 0° and 50°, while the change in angle is slower between 50°–180°. Therefore, the tendency of the angle curve in the unfolding process is to be fast and then slow.

3.2. Mechanical Modeling and Analysis. In the movement of folding and unfolding of wings, the torsion hinge between plate ③ and plate ④ is driven by the motor to fold the wings. *OC* is selected as the rotation axis for torque analysis. The output torque of the motor is affected by the posture of wings and the gravitational forces of the plates. In fact, the movement of plate ① lags behind plate ③, which can be expressed using the dihedral angle $\theta_1 > \theta_3$. The output torque of the motor is given by M; the torque of plates acting about the axis of rotation is M_1, M_2, and M_3. The bending deformation stress of the torsion hinges is given by f_1, f_2, f_3, and f_4, where $f_1 = f_3$ and $f_2 = f_4$. The torque of the torsion hinges acting about the axis of rotation are Mf_1, Mf_2, Mf_3, and Mf_4. The total torque is ΣM_F and the total resistance torque is ΣM_f.

The equilibrium equations for the static analysis of the folding wing movement are as follows:

(1) When the angle $\pi/2 < \theta_3 < \pi$, the total resistance torque is $\Sigma M_{f1} = M_1 + M_2 + M_3 + Mf_1 + Mf_2 + Mf_3 + Mf_4$, the total torque is $\Sigma M_{F1} = M$, and the equilibrium equation is $\Sigma M_{F1} = \Sigma M_{f1}$.

(2) When the angle $\theta_3 < \pi/2$ and $\theta_1 > \pi/2$, the total resistance torque is $\Sigma M_{f2} = M_1 + Mf_1 + Mf_2 + Mf_3 + Mf_4$, the total torque is $\Sigma M_{F2} = M_2 + M_3 + M$, and the equilibrium equation is $\Sigma M_{F2} = \Sigma M_{f2}$.

(3) When the angle $\theta_3 < \pi/2$, the total resistance torque is $\Sigma M_{f3} = Mf_1 + Mf_2 + Mf_3 + Mf_4$, the total torque is $\Sigma M_{F3} = M_1 + M_2 + M_3 + M$, and the equilibrium equation is $\Sigma M_{F3} = \Sigma M_{f3}$.

Figure 6 shows the structure of the fully expanded wings. Figure 7 is a schematic of the state of the wings at $\theta_3 = 135°$. In the folding movement, it is assumed that the center of mass of plate ②, plate ③, and their torsion hinges is at point *B*. Additionally, it is assumed that the center of mass of plate ① and its torsion hinges is at point *F*. Using these assumptions, the distance of *B* and *F* to *OC* can be calculated, respectively, using

$$\begin{aligned}&l_B = \sin\gamma\frac{l - l_{OE}}{\cos(\pi - \gamma - \delta)},\\&l_F = \sqrt{[l_{FE}\sin(\pi - \theta_4)]^2 + \left[\sin\left(\delta - \frac{\pi}{2}\right)\left(\frac{l_{OE}}{\tan(\delta - \pi/2)} - l_{FE}\cos(\pi - \theta_4)\right)\right]^2}.\end{aligned} \tag{4}$$

Figure 8 is a diagram of the stress analysis when the wings are in the state shown in Figure 7 (front view, clockwise deflection 45°). The torque of the plates and torsion hinges relative to the axis *OC* is calculated using

$$M_1 = l_F(G_1 + G_0)\cos(\pi - \theta_4), \tag{5}$$

$$M_2 = l_B(G_2 + G_0)\cos(\pi - \theta_3), \tag{6}$$

$$M_3 = l_B(G_3 + G_0)\cos(\pi - \theta_3), \tag{7}$$

$$Mf_1 = Mf_3 = f_1 l_a + f_1 l_{OA}\sin(\delta - \gamma), \tag{8}$$

$$\begin{aligned}Mf_2 &= Mf_4\\&= f_2 l_{OB}\sin\gamma + f_2\left[\frac{l_{OD}}{2}\sin(\pi - \delta) - l_a\cos(\pi - \delta)\right].\end{aligned} \tag{9}$$

The mechanical analysis of the foldable wings was carried out using the software MATLAB. By analyzing the physical dimensions of the flexible wing of *Allomyrina dichotoma* and considering the output torque of the motor, the structural parameters of the bionic wing were determined, as shown in Table 2.

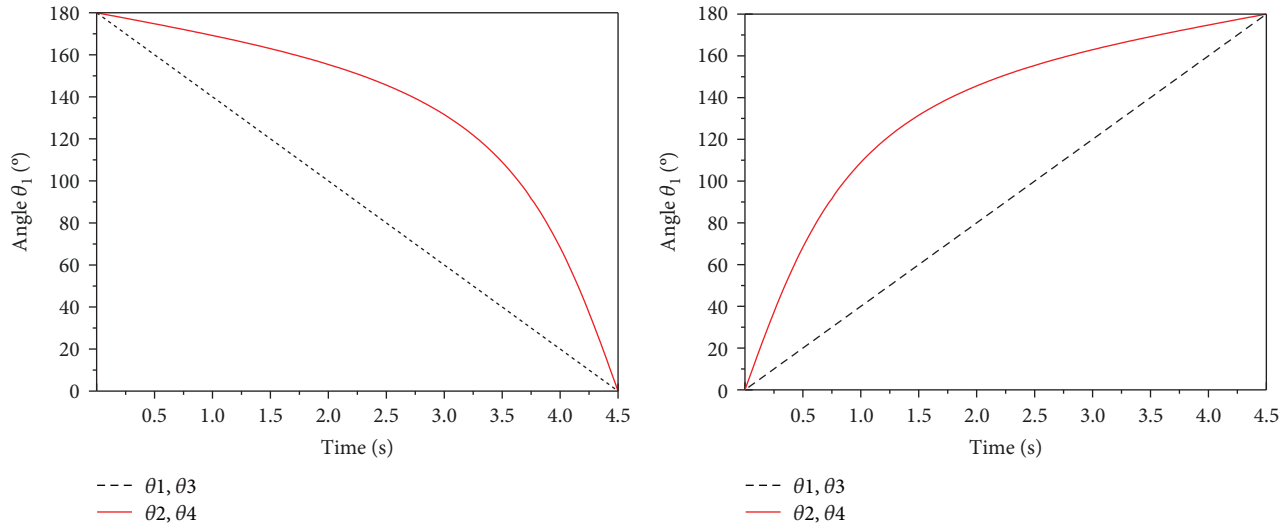

(a) The folding movement

(b) The unfolding movement

Figure 5: The dihedral angle in the folding/unfolding movement.

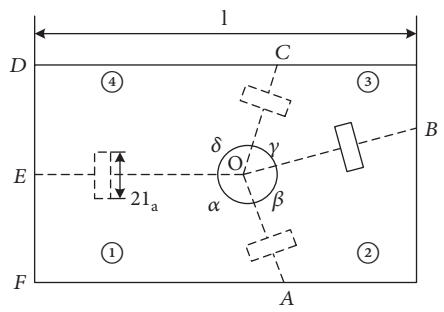

Figure 6: Structure of fully expanded wings.

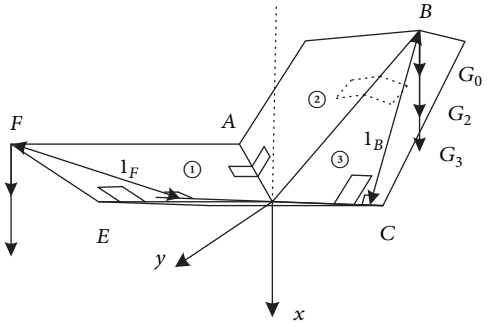

Figure 8: Diagram of stress analysis.

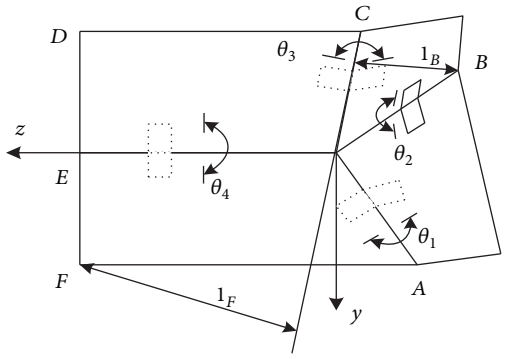

Figure 7: State of wings at $\theta_3 = 135°$.

Table 2: The parameters of wings.

Parameter name	Symbol	Value
Total length	L/mm	60
Total width	$2L_{FE}$/mm	40
Length of OE	L_{OE}/mm	32
Length of hinges	$2L_a$/mm	14
Gravity of plates	G/N	0.2
Gravity of hinges	G_0/N	5×10^{-2}

The creasing angle of the plates greatly influences the output torque of the motor in the movement of wings. The initial output torque of the motor was obtained for different values of γ (80°, 63°, 60°, 55°, 50°, and 40°) and over a range of δ, as shown in Figure 9.

As shown in Figure 9, when $\gamma > 63°$, the curve has a continuous upward slope with increasing δ. When $40° < \gamma \leq 63°$, a local minimum in the output torque of the motor is observed. When $\gamma = 40°$, the output torque of the motor is at a minimum when $\delta = 180°$. When γ is equal to 63°, 60°, 55°, 50°, and 40°, the minimum output torques of the motor are 0.842 N·m, 0.776 N·m, 0.504 N·m, 0.357 N·m, and 0.232 N·m, respectively.

To compare the driven torque required for the wing movements at different γ, the output torque of the motor was simulated with a code implemented in MATLAB. The simulation results are shown in Figure 10. With the

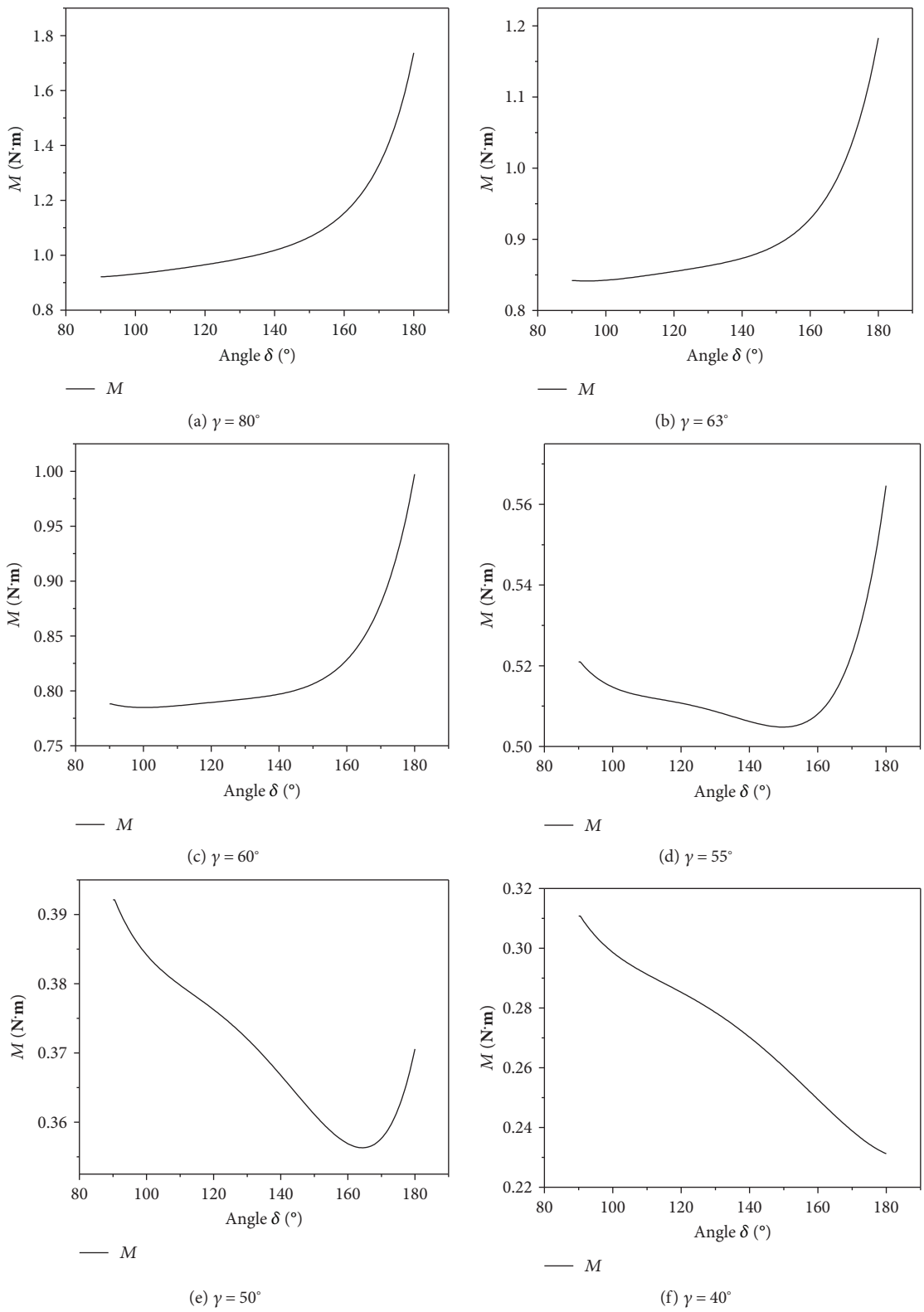

Figure 9: Output torques of the motor in different γ and δ.

decreasing γ, the initial output torque of the motor also decreases. However, after the wings are completely folded, the final output torque of the motor remains unchanged at 2.264 N·m, since the output torque of the motor is primarily affected by the torque of the torsion hinges. The simulation results agree with the results expected in reality.

3.3. Analysis of the Folding Ratio of Wings. The folding ratio refers to the proportion of the existing area or volume to the original area or volume when an object is folded, which reflects the degree of folding. A higher folding ratio indicates a better folding effect. The static analysis model established in the present work ignores the effect of plate thickness, and when the wings are fully folded, the volumetric folding ratio is 100%. Analysis of the folding movement shows that the folding ratio is directly related to the creasing angle of the plates. According to the above analysis, the folding ratio of area for different plate creasing angles can be obtained.

(1) When the angle $\delta = \pi/2$ and $\gamma = \pi/2$, Fr = 75%.

(2) When the angle $\gamma < \pi/2$ and $\pi/2 < \delta < \pi/2 + \arctan((l - l_{OE})/l_{FE})$,

$$\mathrm{Fr} = 1 - \frac{l_{OE} \cdot l_{FE} + (1/2){l_{OE}}^2 \cdot \tan(\delta - \pi/2) + 1/2\{l - [l_{OE} + l_{FE} \cdot \tan(\delta - (\pi/2))]\}^2 \cdot \tan(2\delta - \pi)}{l \cdot 2l_{FE}}. \tag{10}$$

(3) When the angle $\gamma < \pi/2$ and $(\pi/2) + \arctan((l - l_{OE})/l_{FE}) < \delta < \pi$,

$$\mathrm{Fr} = 1 - \frac{l_{OE} \cdot l_{FE} + 1/2(l - l_{OE}) \cdot [2l_{FE} - (l - l_{OE}) \cdot \tan(\pi - \delta)]}{l \cdot 2l_{FE}}. \tag{11}$$

(4) When the angle $\delta = \pi$, Fr = 50%.

The curve of the folding ratio of wings as a function of δ is shown in Figure 11.

Through simulation analysis, it can be seen that when $\gamma > 63^\circ$, it is impossible to calculate the effective minimum output torque of the motor. Therefore, the angles between the fold lines of the wings cannot be determined. The area folding ratio of wings cannot be found either. Using (10), the folding ratio of the area is calculated when γ is set to 63 °, 60 °, 55 °, 50 °, and 40 ° and when δ is 94 °, 100 °, 150 °, 163 °, and 180 °. The results are 72.5%, 69.7%, 57.1%, 53.7%, and 50%, respectively. Assuming that the output torque of the motor can be satisfied, the greater the wing folding ratio, the better the folding effect of the wing. Therefore, priority should be given to the wing folding ratio. Therefore, the creasing angles of the wing are set to $\gamma = 63^\circ$, $\delta = 94^\circ$, $\alpha = 117^\circ$, and $\beta = 96^\circ$.

The torque in the wing folding movement calculated by the MATLAB program is shown in Figure 12. The torque of each plate acting on the axis of rotation are M_1, M_2, and M_3. Initially, the minimum output torque of the motor is $M = 0.937$ N·m. When $90^\circ < \theta_3 < 180^\circ$, the output torque is reduced to 0.732 N·m, at which point M is mainly affected by the gravity of plates ② and ③. When $0^\circ < \theta_3 < 90^\circ$, the output torque of the motor gradually increases to 2.264 N·m. The curve has an inflection point at $\theta_3 = 40^\circ$. When $40^\circ < \theta_3 < 90^\circ$, M is primarily affected by the gravity of plate ①. When $0^\circ < \theta_3 < 40^\circ$, the bending deformation stress of torsion hinges are much greater than the gravity of the plates, and M is mainly affected by bending deformation of torsion hinges. As such, when $0^\circ < \theta_3 < 40^\circ$, M increases faster. The curves of Mf_1 and Mf_2 in the figure show the moment of the elastic hinge with respect to the rotation axis. As the wings are folded, the deformation of the elastic hinge increases continuously and the force of the elastic hinge increases accordingly. As such, the resistance moment to the wing folding motion increases, which is expected.

4. Motion Simulation of Folding Wing

A 3D model of the bionic wing was established using SolidWorks software. The model was imported into ADAMS, and constraints and material properties were added. The driven functions based on the static analysis and the desired folding motion were also applied. The simulation type and step size and contact parameters based on known material properties were also set.

For the folding motion of bionic wings, the flexible deformation characteristics of the wings must be taken into account. In the present work, the model was processed with flexibility using ADAMS. The uniform velocities in the folding/unfolding movements were compared for two types of wings.

The simulation of the wing folding movement is shown in Figure 13. The driven force acts on the axis of rotation between plates ④ and ③, so that plate ③ moves toward plate ④. As the plates are all connected by torsion hinges, the rest of the plates are driven by the motion of plate ③, ultimately achieving the folding movement.

After the simulation, the movement parameters of the wings under different conditions can be measured using the ADAMS postprocessor. Figure 14(a) shows the dihedral angle of the rigid wings. Figure 14(b) shows the dihedral angle of the flexible wings. The maximum deviation of the dihedral angle of the two types of wings is shown in Table 3. From Figures 5 and 14(a), it can be seen that the dihedral angle obtained by the kinematic mathematical model is consistent with the result of ADAMS simulation. The trends of the curves are both first slow and then fast. The observed inflection point is found at 131° and 133°, respectively. The inflection point error between the two methods is 1.53%. Compared with rigid wings, the flexible wings cannot be completely folded. The maximum deviation of the dihedral angle of the two types of wings is $\Delta\theta_4 = 24.4^\circ$, $\Delta\theta_2 = 19.1^\circ$, $\Delta\theta_1 = 14.2^\circ$, and $\Delta\theta_3 = 0^\circ$. The corresponding deviation ratios are 13.5%, 10.6%, 7.9%, and 0,

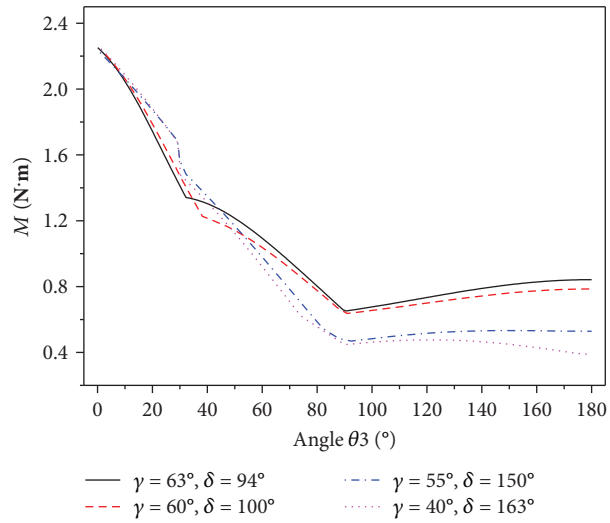

Figure 10: Output torque of the motor in different γ.

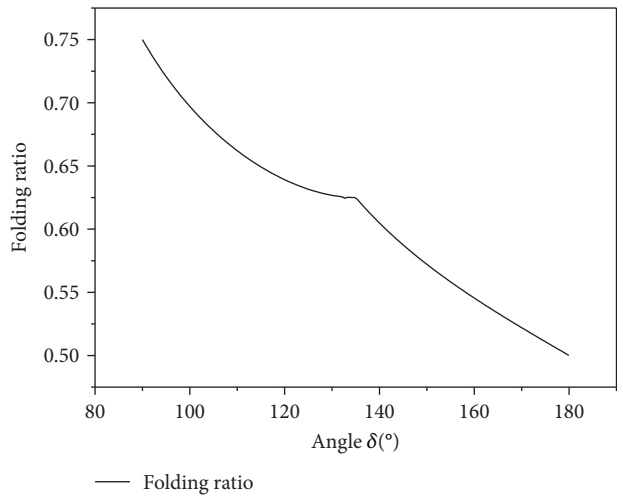

Figure 11: Folding ratio in different δ.

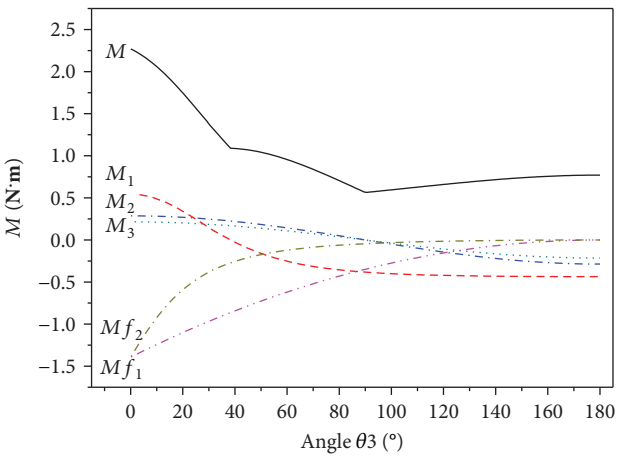

Figure 12: Torque of plates and torsion hinges.

respectively. From Table 3 and the kinematic model, it can be seen that when the wings are in the folded state, plate ① and plate ④ are on the outside in the folded direction and the dihedral angle between plates ① and ④ should be the largest. Therefore, $\Delta\theta_4$ has a greater impact on the folding ratio of the wings. The smaller the value of $\Delta\theta_4$, the greater the volumetric folding ratio of the wings.

The torque of the torsion hinges of the wings in the folding/unfolding motion was obtained from the simulation, as shown in Figure 15. The deviation in the maximum torque of the torsion hinges for the two types of wings is shown in Table 4. The maximum torque is $Mf = 0.539$ N·m. The deviations in the torque of torsion hinges of the two types of wings are $\Delta Mf_3 = 0$ N·m, $\Delta Mf_1 = 0.14$ N·m, $\Delta Mf_2 = 0.26$ N·m, and $\Delta Mf_4 = 0.3$ N·m. The deviation ratios are 0, 9.3%, 17.2%, and 19.9%, respectively. From Table 4 and the analysis of statics, we can obtain the stiffness and other physical parameters of torsion hinges that affect the output torque of the motor. The smaller the stiffness of the torsion hinges, the smaller the maximum output torque of motor.

5. Conclusion

(1) A calculation model of the folding ratio for folding wing is established in this paper. According to the analysis of the wing folding ratio, the creasing angles of the plates of the bionic foldable wings are $\gamma = 63^\circ$, $\delta = 94^\circ$, $\alpha = 117^\circ$, and $\beta = 96^\circ$.

(2) According to the kinematics of the bionic foldable wings, the dihedral angles between each fin plate are calculated. The results are compared with ADAMS dynamic simulation data, and the inflection point error between the two is 1.53%. This illustrates that the theoretical calculation is consistent with the simulation. Additionally, it proves that the design of the folding mechanism is reasonable.

(3) The output torque of the motor is obtained by mechanics calculation and simulation. It shows that the smaller the stiffness of the torsion hinges, the smaller the maximum output torque of motor.

(4) The results from simulating two types of wings show that the folding ratio of flexible wings in the fully folded state is less than that of the rigid wings. From the simulation and analysis, it was found that $\Delta\theta_4$ has a greater impact on the folding ratio of wings. The smaller the value of $\Delta\theta_4$, the greater the volumetric folding ratio of the wings. It is possible that in addition to the main motor, a motor could be added on the revolute pair between plates ① and ④. At the end of the folding process, the additional motor would drive plate ① to move closer to plate ④, which would achieve the purpose of reducing $\Delta\theta_4$ and subsequently increase the folding ratio of the wings. It provides

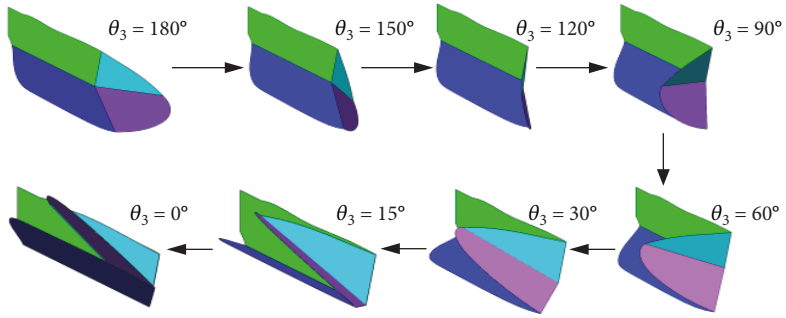

Figure 13: Folding movement of wings.

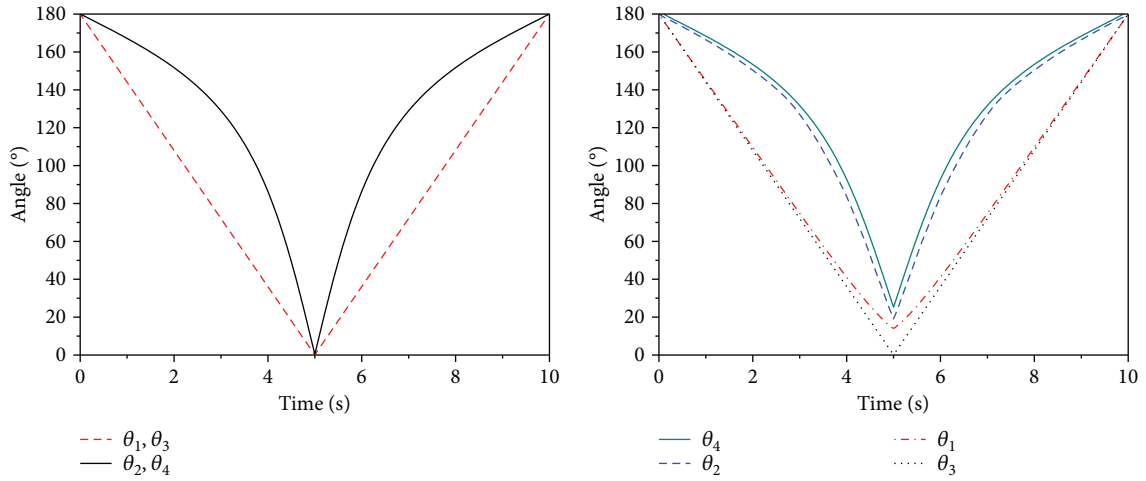

(a) Rigid wings (b) Flexible wings

Figure 14: Dihedral angle of wings in the folding/unfolding motion.

Table 3: The maximum deviation of the dihedral angle.

	$\Delta\theta_4$	$\Delta\theta_2$	$\Delta\theta_1$	$\Delta\theta_3$
The deviation of the dihedral angle	24.4°	19.1°	14.2°	0°

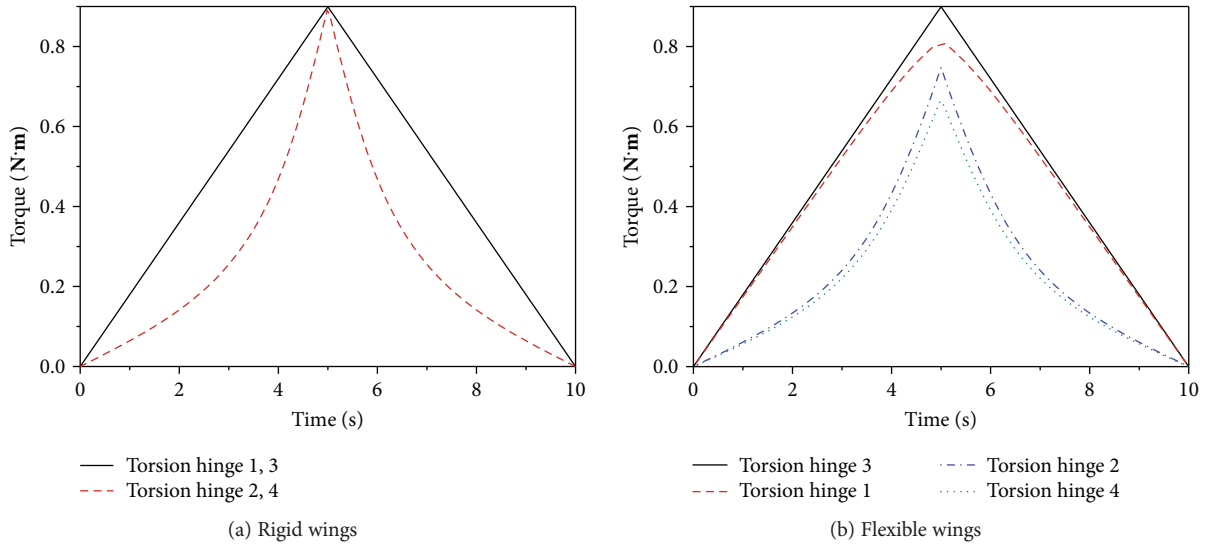

(a) Rigid wings (b) Flexible wings

Figure 15: Torque of torsion hinges of wings.

Table 4: The difference in the maximum torque of the two types of wings.

	ΔMf_4	ΔMf_1	ΔMf_2	ΔMf_3
The difference of the torque	0.182 N·m	0.087 N·m	0.160 N·m	0 N·m

a basis for optimizing the design of the parameters of the folding wing.

Data Availability

The data used to support the findings of this study are available from the corresponding author upon request.

Conflicts of Interest

The authors declare that they have no conflicts of interest.

Acknowledgments

This work is sponsored by the National Natural Science Foundation of China (Grant no. 51705473), Natural Science Foundation of Henan Province (Grant no. 162300410316), Youth Backbone Teachers Training Plan of Henan Province Colleges (Grant no. 2016GGJS-089), and the Open Project of Henan Key Laboratory of Intelligent Manufacturing of Mechanical Equipment (IM201806).

References

[1] R. Madangopal, Z. A. Khan, and S. K. Agrawal, "Energetics-based design of small flapping-wing micro air vehicles," *IEEE/ASME Transactions on Mechatronics*, vol. 11, no. 4, pp. 433–438, 2006.

[2] R. B. R. Vandenheede, L. P. Bernal, C. L. Morrison et al., "Experimental and computational study on flapping wings with bio-inspired hover kinematics," *AIAA Journal*, vol. 52, no. 5, pp. 1047–1058, 2014.

[3] W. B. Tay, "Effect of different types of wing-wing interactions in flapping MAVs," *Journal of Bionic Engineering*, vol. 14, no. 1, pp. 60–74, 2017.

[4] J. Young, J. C. S. Lai, and M. F. Platzer, "A review of progress and challenges in flapping foil power generation," *Progress in Aerospace Sciences*, vol. 67, pp. 2–28, 2014.

[5] J. Young, S. M. Walker, R. J. Bomphrey, G. K. Taylor, and A. L. Thomas, "Details of insect wing design and deformation enhance aerodynamic function and flight efficiency," *Science*, vol. 325, no. 5947, pp. 1549–1552, 2009.

[6] J. Zhu and T. Tian, "The time asymmetric pitching effects on the energy extraction performance of a semi-active flapping wing power generator," *European Journal of Mechanics - B/Fluids*, vol. 66, pp. 92–101, 2017.

[7] J. Sun, M. Ling, W. Wu, B. Bhushan, and J. Tong, "The hydraulic mechanism of the unfolding of hind wings in *Dorcus titanus platymelus* (order: Coleoptera)," *International Journal of Molecular Sciences*, vol. 15, no. 4, pp. 6009–6018, 2014.

[8] X. Ke, W. Zhang, X. Cai, and W. Chen, "Wing geometry and kinematic parameters optimization of flapping wing hovering flight for minimum energy," *Aerospace science and Technology*, vol. 64, no. 12, pp. 192–203, 2017.

[9] A. Muhammad, Q. V. Nguyen, H. C. Park, D. Y. Hwang, D. Byun, and N. S. Goo, "Improvement of artificial foldable wing models by mimicking the unfolding/folding mechanism of a beetle hind wing," *Journal of Bionic Engineering*, vol. 7, no. 2, pp. 134–141, 2010.

[10] Q.-T. Truong, B. W. Argyoganendro, and H. C. Park, "Design and demonstration of insect mimicking foldable artificial wing using four-bar linkage systems," *Journal of Bionic Engineering*, vol. 11, no. 3, pp. 449–458, 2014.

[11] Z. Rui, A. Haisong, M. Yuan, and J. Jian, "Flexiblity of flapping wing and its effect on aerodynamic characteristic," *Chinese Journal of Computational Mechanics*, vol. 22, no. 6, pp. 750–754, 2005.

[12] Z. Zhenjun, L. Haibo, and B. Guo, "The coupled flight dynamic and structural dynamic method for the flexible flight vehicle," *Missiles and Space Vehicles*, no. 3, pp. 11–14, 2012.

[13] P. Cheng, *Insect Motion Parameters and Optical Measurement and Demonstration of Wing Deformation in Flight*, University of Science and Technology of China, 2007.

[14] N. S. Ha, T. L. Jin, N. S. Goo, and H. C. Park, "Anisotropy and non-homogeneity of an *Allomyrina Dichotoma* beetle hind wing membrane," *Bioinspiration & Biomimetics*, vol. 6, no. 4, article 046003, 2011.

[15] J. K. Shang, S. A. Combes, B. M. Finio, and R. J. Wood, "Artificial insect wings of diverse morphology for flapping-wing micro air vehicles," *Bioinspiration & Biomimetics*, vol. 4, no. 3, article 036002, 2009.

[16] M. Ghommem, N. Collier, A. H. Niemi, and V. M. Calo, "On the shape optimization of flapping wings and their performance analysis," *Aerospace Science and Technology*, vol. 32, no. 1, pp. 274–292, 2014.

[17] W. B. Tay, "Symmetrical and non-symmetrical 3D wing deformation of flapping micro aerial vehicles," *Aerospace Science and Technology*, vol. 55, pp. 242–251, 2016.

[18] J. Bluman and C. K. Kang, "Achieving hover equilibrium in free flight with a flexible flapping wing," *Journal of Fluids and Structures*, vol. 75, pp. 117–139, 2017.

[19] F. Haas and R. J. Wootton, "Two basic mechanisms in insect wing folding," *Proceedings of the Royal Society B: Biological Sciences*, vol. 263, no. 1377, pp. 1651–1658, 1996.

[20] F. Haas and G. B. Rolf, "Wing folding and the functional morphology of the wing base in Coleoptera," *Zoology*, vol. 104, no. 2, pp. 123–141, 2001.